Molecular Therapy
Methods & Clinical Development
Original Article

Gene therapy using an ortholog of human fragile X mental retardation protein partially rescues behavioral abnormalities and EEG activity

Alexander W.M. Hooper,[1,4] Hayes Wong,[1,4] Yosuke Niibori,[1] Rozita Abdoli,[1] Subha Karumuthil-Melethil,[2] Chunping Qiao,[2] Olivier Danos,[2] Joseph T. Bruder,[2] and David R. Hampson[1,3]

[1]Leslie Dan Faculty of Pharmacy, Department of Pharmaceutical Sciences, University of Toronto, Toronto, Ontario, Canada M5S 3M2; [2]Research and Early Development, REGENXBIO Inc. Rockville, Maryland, U.S.A. 20850; [3]Department of Pharmacology and Toxicology, Faculty of Medicine, University of Toronto, Toronto, Ontario, Canada M5S 3M2

Fragile X syndrome (FXS), a neurodevelopmental disorder with no known cure, is caused by a lack of expression of the fragile X mental retardation protein (FMRP). As a single-gene disorder, FXS is an excellent candidate for viral-vector-based gene therapy, although that is complicated by the existence of multiple isoforms of FMRP, whose individual cellular functions are unknown. We studied the effects of rat and mouse orthologs of human isoform 17, a major expressed isoform of FMRP. Injection of neonatal *Fmr1* knockout rats and mice with adeno-associated viral vectors (AAV9 serotype) under the control of an MeCP2 mini-promoter resulted in widespread distribution of the FMRP transgenes throughout the telencephalon and diencephalon. Transgene expression occurred mainly in non-GABAergic neurons, with little expression in glia. Early postnatal treatment resulted in partial rescue of the *Fmr1* KO rat phenotype, including improved social dominance in treated *Fmr1* KO females and partial rescue of locomotor activity in males. Electro-encephalogram (EEG) recordings showed correction of abnormal slow-wave activity during the sleep-like state in male *Fmr1* KO rats. These findings support the use of AAV-based gene therapy as a treatment for FXS and specifically demonstrate the potential therapeutic benefit of human FMRP isoform 17 orthologs.

INTRODUCTION

Fragile X syndrome (FXS) is a genetic disorder caused by a CGG-triplet-repeat expansion near the promoter region of the X-linked *FMR1* gene. FXS is the most common single-gene cause of cognitive impairment and autism, affecting approximately 1 in 5,000 men and about 1 in 8,000 women.[1,2] The triplet-repeat expansion causes partial or complete inhibition of production of the encoded protein, fragile X mental retardation protein (FMRP), thereby inducing cognitive impairment and autism or autism-related behaviors. Pharmacotherapeutic treatments, such as stimulants, antidepressants, and antipsychotics, suppress the symptoms but induce side effects and do not address the underlying cause of the disorder. Viral-vector-mediated gene therapy using adeno-associated viral (AAV) vectors represents a different therapeutic approach, which could potentially convey a more comprehensive and long-term correction of the underlying pathology.[3]

We and others have reported the results of AAV gene-therapy experiments using the *Fmr1*-knockout (KO) mouse model of FXS.[4–6] Each of these studies reported partial reversal of abnormal biochemistry, physiology, and/or behaviors. One shortcoming of all previous efforts was that the full-length isoform of FMRP was studied (isoform 1). Alternative splicing of the *FMR1* gene is complex and results in at least 15 mRNA isoforms expressed in human and rodent cells and tissues.[7–11] Based on mRNA expression experiments, isoform 1 is now known to be a relatively minor isoform. Isoforms lacking exon 12 (which contains part of the sequence for the RNA-binding K homology domain KH2) appear to constitute most of the FMR1 mRNAs in human brain tissue samples. The most highly transcribed of these exon-12-lacking isoforms are isoforms 7 and 17, with isoform 17 having the highest transcript levels.[11] These two isoforms differ in the splicing of exon 17, where a 17 amino acid section is removed from isoform 17. This 17 amino acid region is known to be involved in localizing FMRP to Cajal bodies in isoforms lacking exon 14 (e.g., isoform 6) and is not observed in the mouse or rat.[12] Isoform 17 retains most of the functional domains of FMRP, including the Tudor domains, nuclear localization sequence, K homology domains, nuclear exit sequence, and the RGG domain.[11] Being an evolutionarily conserved isoform, as well as having the most-dominant transcript levels in the brain, isoform 17 is an excellent candidate for a single isoform expressing the therapeutic vector for FXS treatment.

Genetically modified rats are an alternative to mouse models and may have some advantages including larger brain size and a higher level of cognitive abilities.[13,14] We recently characterized the phenotype of a

Received 20 January 2021; accepted 30 June 2021;
https://doi.org/10.1016/j.omtm.2021.06.013.

[4]These authors contributed equally

Correspondence: David R. Hampson, PhD, Department of Pharmaceutical Sciences, Leslie Dan Faculty of Pharmacy, Univerity of Toronto, ON M5S 3M2, Canada.
E-mail: d.hampson@utoronto.ca

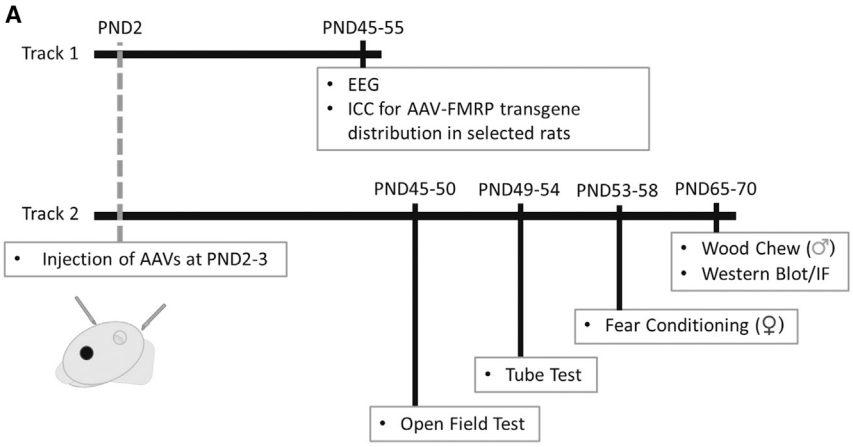

Figure 1. Timeline of behavioral and physiological analyses

Rats were injected via ICV and ICM at PNDs 2–3 and assigned to either EEG (track 1) or behavior analyses (track 2). Samples for western blots and immunocytochemical analyses were collected at PNDs 30 and 70.

fragile X KO rat in which an emphasis was placed on comparing male and female KO rats and assessing behavioral parameters that could be potentially translatable to clinical studies in humans.[15] The present study is the first to assess viral vector gene therapy in the *Fmr1* KO rat model of FXS. We used the rat homolog of human isoform 17 (rat isoform X3), a highly abundant isoform.[10,11] We demonstrate correction of several key autism-related behaviors and encephalogram (EEG) patterns in the *Fmr1* KO rat, further establishing the efficacy of AAV-mediated expression of FMRP as a potential long-lasting therapeutic treatment for FXS.

RESULTS

The overall study design and timelines are outlined in Figure 1. The animals were treated by combined intra-cerebroventricular (ICV) and intra-cisterna magna (ICM) cerebrospinal fluid (CSF) injections on postnatal day (PND) 2 or 3. Brain samples for western blot and immunocytochemical analyses were collected between PNDs 30 and 70, depending on the experiment, as indicated in the figure legends. All samples were age-matched.

AAV vectors and transduction efficacy

Based on studies of human *FMR1* mRNA, we predicted that the rat and mouse homologs of human isoform 17 (rat X3 and mouse isoform 7) correspond to highly expressed isoforms in rodent brain.[11] Schematic representations of the rat and mouse vectors used are shown in Figure 2A. Human isoform 17, and the rat X3 and mouse isoform 7 homologs, differ from full-length isoform 1 by the exclusion of exon 12. To verify that rat X3 and mouse isoform 7 are major expressed isoforms, *Fmr1* KO rats were injected with AAV-X3, and KO mice were injected with AAV-iso7 via combined ICV and ICM injection, and frontal cortex lysates from those animals were compared with wild-type (WT) controls. Western blotting showed that the molecular weight of the rat X3 transgene protein corresponded in size to the most abundantly expressed isoform of FMRP in WT rat brain (Figure 2B). This was also true for the frontal cortex lysates in mice, in which transgene expression of mouse FMRP isoform 7 produced a protein that co-migrated with the most highly expressed isoform of FMRP in WT mice (Figure 2C).

Based on our previous work in the *Fmr1* KO mouse,[6] because of the ineffectiveness of the under-expressing FMRP and the detrimental effects of massively overexpressing FMRP, one goal of the present study was to create an AAV vector that would induce FMRP expression at a level similar to that of the WT. Because of the limited space available in an AAV vector, and the fact that a compact version of the *Fmr1* promoter has not been identified, we employed a mini-MeCP2 promoter to drive FMRP expression. The rationale was based on a general pattern of co-expression of FMRP and the transcription regulator MeCP2 in neurons and on the recently documented inter-regulation between the two proteins.[16]

Using western blotting, we observed that at PND 30 in the frontal cortex of AAV-X3 injected rats, the expression level of the X3 transgene was higher than the combined expression of all of the endogenously expressed isoforms of FMRP in the WT. However, X3 expression declined by PND 70 (Figures 2D and 2E). Although at PND 70, expression declined to approximately half the value of the total endogenous FMRP, it is important to note that, in the western blot analysis, X3 levels in the KOs were compared with the natural expression of multiple FMRP isoforms in the WT, which may not have been fully resolved by gel electrophoresis. By comparison, expression in the dissected whole hippocampus of injected rats was significantly lower than FMRP expression in the hippocampus of WT rats at PND 30 (Figure 2D). This may be explained, in part by the fact that although the dorsal hippocampus is close to the AAV injection site in the ventricle, the ventral hippocampus extends some distance distal from the injection site.

FMRP is endogenously expressed throughout the CNS and, therefore, ideally, AAV-mediated FMRP expression would mimic that widespread brain distribution. We observed a similar overall pattern of transgene expression in AAV-X3-injected rats (Figures 3A and 3B) and AAV-iso7-injected mice (Figure S1). For both rodent species, expression was high in the motor and frontal cortices, moderate in the hippocampus and in the striatum of the rat and the thalamus of the mouse. Low-transgene expression was seen in the superior colliculus and inferior colliculus of the mouse and in the cerebellum and brainstem of both mice and rats.

Cell-type specificity and coverage

Because FMRP is expressed in most CNS neurons, we aimed to transduce as many neuronal populations as possible, while limiting

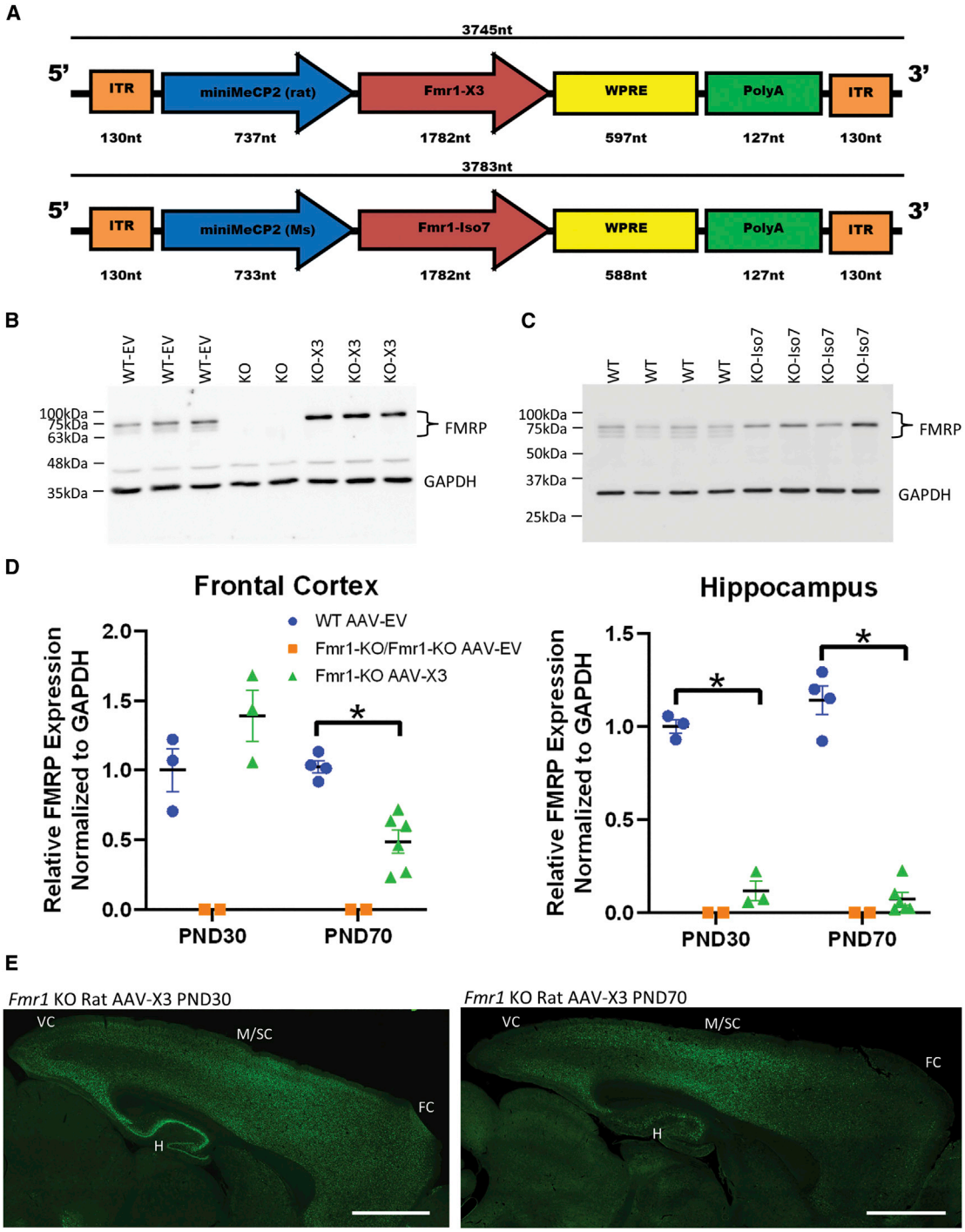

Figure 2. Expression of FMRP transgenes in the CNS of rats and mice

(A) Schematic depiction of the AAV9 vectors. WPRE, woodchuck hepatitis virus posttranscriptional regulatory element; PolyA, polyadenylation region. The relative molecular weights of proteins expressed from the AAV-X3 and AAV-Iso7 vectors correspond with the most highly expressed FMRP isoforms in the young adult (PNDs 60–70) frontal cortex of both rats (B) and mice (C). (D) FMRP-X3 transgene expression in *Fmr1* KO rats at PND 30 is similar to total isoform FMRP expression in the frontal cortex of WT rats but is reduced by PND 70. Expression of FMRP-X3 in the hippocampus of rats was significantly less than that of WT rats at PND 30 and PND 70. Error bars are means ± SEM. *$p < 0.05$, 1-way ANOVA, Tukey's post hoc. n values are the number of animals analyzed: PND 30: WT AAV-EV = 3, *Fmr1* KO AAV-EV = 2, *Fmr1* KO AAV-X3 = 3; PND 70: WT AAV-EV = 4, *Fmr1* KO AAV-EV = 2, *Fmr1* KO AAV-X3 = 5. (E) Representative images of FMRP-X3 protein in the rat at PND 30 and PND 70. Expression of the transgene was present in the visual cortex (VC), motor cortex, and somatosensory cortex (M/SC), frontal cortex (FC), and hippocampus (H), at both ages. Scale bars, 2 mm.

A

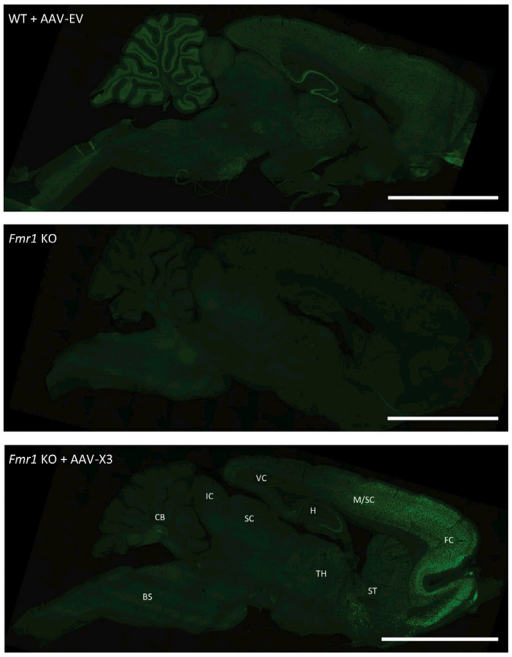

B

	AAV9-X3
Dose (total vg)	1.02x10E12
Prefrontal Cortex	+++
Motor/Somatosensory Cortex	+++
Visual Cortex	++
Hippocampus	++
Striatum	++
Thalamus	+
Superior Colliculus	-
Inferior Colliculus	-
Cerebellum Molecular Layer	-
Cerebellum Purkinje Layer	+
Cerebellum Granular Layer	-
Brain Stem	+
No Expression	-
Sparse/Low Expression	+
Moderate Expression	++
High/Complete Expression	+++

Figure 3. AAV9-expressed transgene distribution

(A) Representative expression of FMRP-X3 protein in the rat and FMRP-iso7 protein in the mouse at PND 30 after ICV + ICM injection of AAV9s at PND 2. Immunofluorescent imaging of the rat brain revealed high expression in the motor and somatosensory cortex (M/SC) and frontal cortex (FC), with moderate expression in the hippocampus (H), visual cortex (VC), thalamus (TH), and striatum (ST). FMRP was detected in these same regions in mice injected with FMRP-iso7 and, additionally, in the inferior colliculus (IC) and superior colliculus (SC). FMRP was very low in the brainstem (BS) and cerebellum (CB) in injected rats and mice. (B) Summary of semiquantitative analysis of relative expression levels in AAV-X3 treated rats. Rating scale: +++, high expression; ++, moderate expression; +, low expression; −, negligible expression; vg, AAV vector genomes injected. Scale bars, 5 mm for rat, and 2 mm for mouse.

expression in glia because levels of FMRP in the glia are low in the mature mouse brain.[17] As observed in WT neurons, higher-magnification images illustrate that intracellular expression of FMRP from both rat AAV-X3 (Figures 4A and 4B) and mouse AAV-iso7 (Figures S1 and S2) was mainly localized to the cytosol of the neurons. As observed in the WT rat brain, anti-FMRP immunoreactivity in neuronal cell bodies was present as dense granules (Figure 4A), and neuronal processes were also immuno-labeled in *Fmr1* KO rats injected with AAV-X3 (Figure 4B). These results indicate that the AAV-FMRP-X3 transgene displayed an intracellular distribution that was similar to that of the WT controls.

Analysis of the cell-type specificity of the X3 transgene in 9 week-old KO rats demonstrated that expression was primarily in $NeuN^+$ neurons, with more than 90% of transduced neurons in the cortex and more than 96% of the transduced neurons in the hippocampus being $NeuN^+$. This was similar to the proportions of $FMRP^+$ cells seen in WT-empty vector (EV) controls in the same brain regions (Figure 4E). Approximately 60% of $NeuN^+$ neurons expressed the transgenic FMRP in the frontal cortex, with 68% in the motor cortex of injected rats (Figure 4D). Substantially fewer parvalbumin (PV^+) GABA interneurons showed detectable levels of FMRP in the same regions (25% and 20%, respectively; Figure 4F). PV^+ neurons were a small proportion of the $FMRP^+$ cells in the cortex and hippocampus of Fmr1 KO rats injected with AAV-X3; however, this was similar to the proportions of $FMRP^+$ cells types seen in WT-EV controls (Figure 4G). In hippocampal CA1 and CA3 regions, 30%–47% of $NeuN^+$ and 35%–40% PV^+ neurons expressed AAV-X3. A similar expression pattern was observed in mice, with 93%–95% of AAV-Iso7 localized to $NeuN^+$ neurons, and 18%–27% localized to $GAD65/67^+$ GABA interneurons throughout the cortex and hippocampus (Figure S2). In mice, 93%–95% of AAV-Iso7 was localized to $NeuN^+$ neurons and 18%–27% of the expression in $GAD65/67^+$ GABA interneurons throughout the cortex and hippocampus (Figure S2). Quantitation of co-labeled cells with anti-FMRP and anti-S100B, a marker for astrocytes and some oligodendrocyte precursor cells (as described by Gholizadeh et al.[17]), indicated that virtually no $S100\beta^+$ cells co-expressed AAV-Iso7, indicating that glial expression was very low (Figure S2). Thus, the low level of expression of the FMRP isoform 7 transgene in the glia of the young-adult CNS is consistent with the natural pattern of expression of FMRP in the WT brain[17]. Although improvements could be achieved in transduction levels, the described mini-MeCP2 promoter appears to express FMRP in an overall pattern similar to that of the WT controls.

Status of glia and absence of FMRP in the liver of *Fmr1* KOs after treatment

Although the safety of AAVs has been studied extensively, there could be an immunological reaction to the FMRP transgene product itself in the *Fmr1* KO rat. To examine that, we chose to use species-appropriate protein sequences, to inject at a young age, and to inject directly into the CSF to limit an immune response to the transgene. To assess immune activation, we studied activation of the glia cells by performing western blot analysis on frontal cortex lysates from uninjected WT rats, WT rats injected with AAV-EV, uninjected *Fmr1* KO rats, and *Fmr1* KO rats injected with AAV-X3; this analysis was conducted on samples collected at PND 30, corresponding with the peak of transgene expression (Figure 2D). The blots were probed for the activated astrocyte marker glial fibrillary acidic protein (GFAP; Figure 5A) and the activated microglial marker ionized calcium-binding adaptor molecule 1 (Iba1; Figure 5B). No significant differences were found in glial activation between any of the genotypes or treatments, indicating that neither the AAV itself nor the FMRP transgene induced a significant immune response in the brain. The absence of

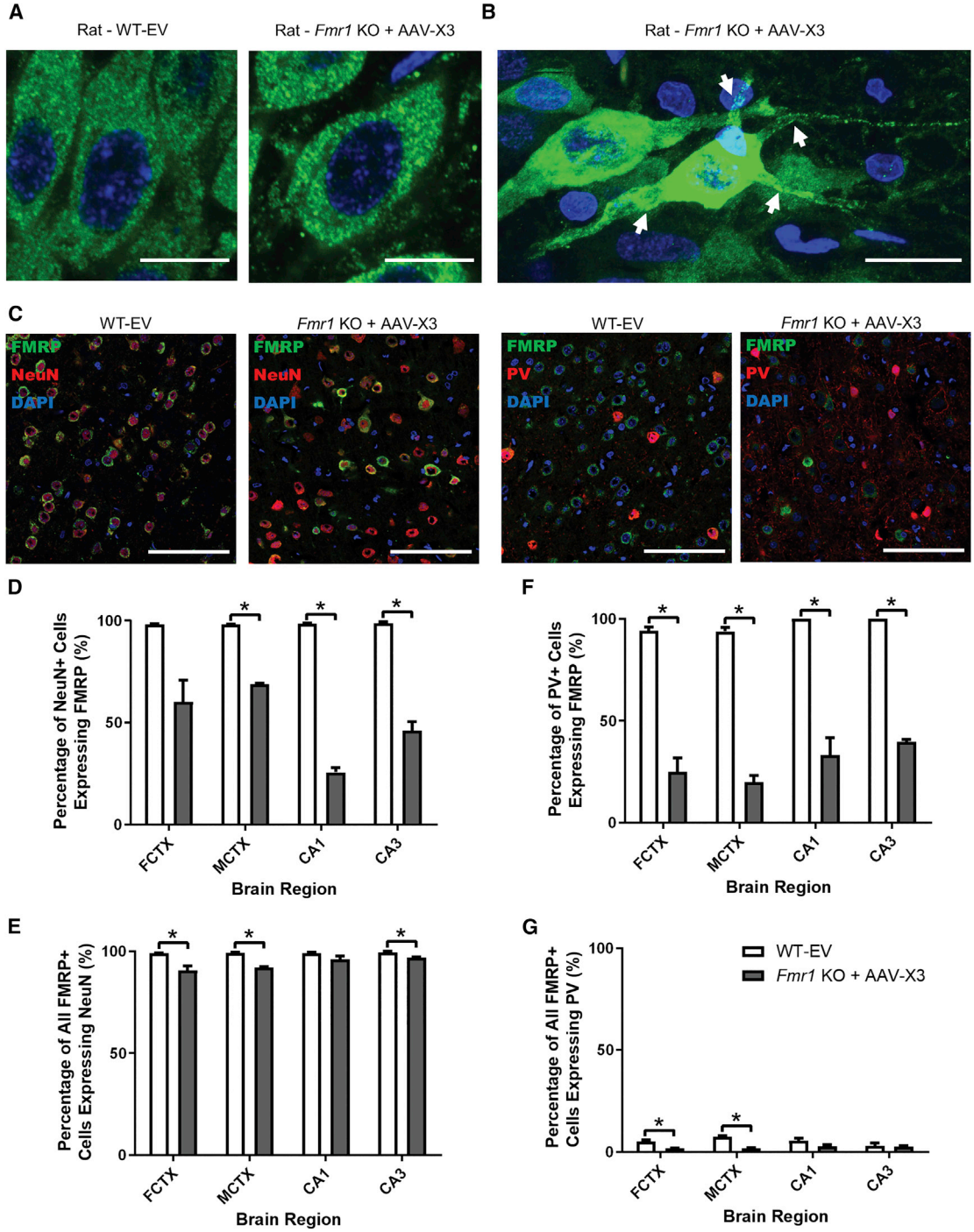

Figure 4. Cytological analysis of FMRP transgene expression

(A) Immunofluorescent staining for FMRP reveals expression of FMRP-X3 in the CA3 region of the hippocampus from *Fmr1* KO rats. Scale bars, 10 μm. (B) Neurons of the CA3 region of the hippocampus from *Fmr1* KO rats injected with FMRP-X3, demonstrating expression of the transgene in the processes of the cell (arrows). Projection from z stack, scale bar, 20 μm. (C–G) Cell-type specificity and coverage of FMRP in WT-EV rats and *Fmr1* KO rats after treatment with AAV-X3. Scale bars, 100 μm. Tissue was labeled for FMRP and co-labeled for NeuN (neurons) (C, D, and E), or parvalbumin (PV, interneurons) (C, F,G), and quantified for co-expression of markers. Error bars are SEM, N = 3 for all groups, *$p < 0.05$ (t test or Welch's t test when appropriate). FCTX, frontal cortex; MCTX, motor cortex; CA1, hippocampus CA1 region; CA3, hippocampus CA3 region.

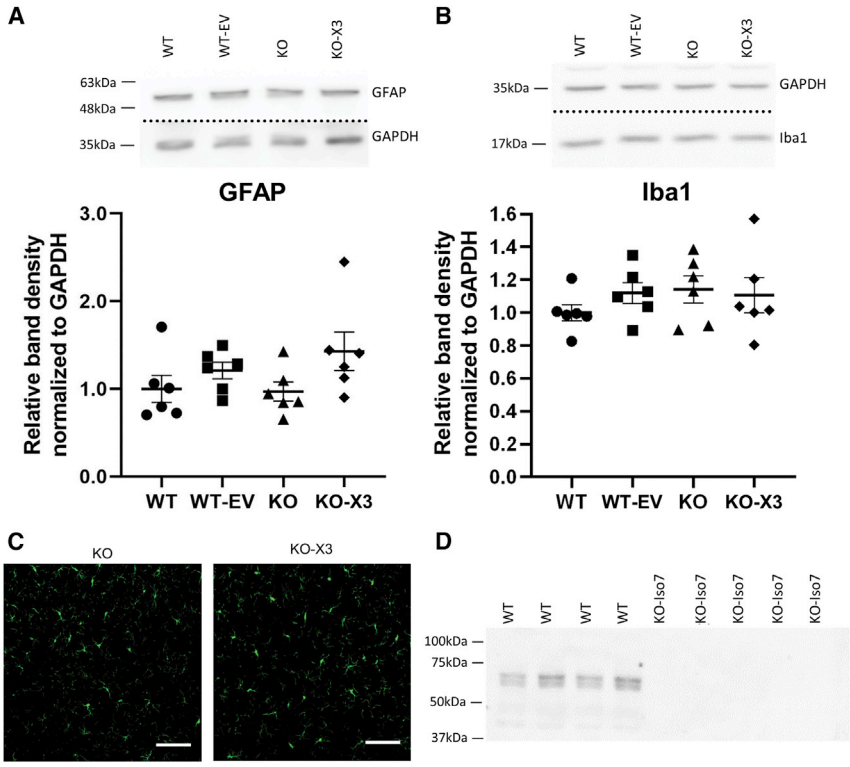

Figure 5. Glial response to AAV-X3 treatment

(A) Western blot of anti-GFAP and quantitation in rat frontal cortex showing no significant activation of astrocytes in AAV-X3-injected rats at PND 30. (B) Western blot and quantitation of Iba-1 in microglia of the frontal cortex of AAV-X3-injected rats at PND 30. N = 6 rats for all groups; error bars are means ± SEM. *$p < 0.05$, one-way ANOVA, Tukey's post hoc. (C) Example of frontal cortex of PND 30 *Fmr1* KO rat injected with AAV-X3 and labeled with anti-Iba-1 showing no activation of microglia. Scale bars, 100 μm. (D) Western blot of liver tissue from PND 30 mice injected with AAV9-Iso7 on PND 2 demonstrating no detectable FMRP transgene expression.

elevated microglia activity was also demonstrated using immunocytochemistry (Figure 5C). Using western blot analysis, we examined liver tissue from PND 25–30 *Fmr1* KO mice injected with AAV-Iso7 (Figure 5D); no FMRP was observed in the liver, indicating that intra-CSF injection of the vector did not result in detectable FMRP transgene expression in that organ.

Electroencephalography analyses

The location of the EEG probes and a schematic diagram of the EEG recording setup are shown in Figures S3A and S3B, and representative EEG traces during the awake and sleep-like states from the three treatment groups are illustrated in Figure S3C. An increase in gamma frequency power is the most consistently reported EEG abnormality in both *Fmr1* KO mice and in patients with FXS.[18–21] In our previous study of *Fmr1* KO rats, this was observed in the male KO rats but not in the females.[15] Therefore, EEG recordings were conducted only in male KO rats in the current study. A comparison of the EEG power among WT-EV, KO-EV, and KO-X3 across all frequency bands during the immobile awake and sleep-like states is shown in Figure 6A. Significant differences between WT-EV and KO-EV and between WT-EV and KO-X3 were observed by two-way ANOVA (genotype; treatment) in both the awake and sleep-like states, and higher gamma frequency power during the sleep-like state was found in both KO-EV and KO-X3 groups by post hoc analysis ($p < 0.05$). This increase in gamma power was consistent with previous results from uninjected *Fmr1* KO rats.[15,22] An increase in gamma power in the awake immobile state was also observed in the KO-X3 group ($p < 0.05$). No significant differences between the KO-EV and KO-X3 groups were observed ($p > 0.05$). This result suggested AAV-X3 treatment had no effect on the abnormal gamma oscillations found in the *Fmr1* KO rats.

Also consistent with our previous findings,[15] an increase in the range of delta wave activity (1–2 Hz) during the sleep-like state was observed in the WT-EV group when compared with the awake immobile state (two-way ANOVA by frequency and post hoc Sidak multiple comparison; $p < 0.05$), and that increase was not observed in the KO-EV group (Figure 6B). After gene therapy treatment with the AAV-X3 vector, that increase in delta wave activity was restored in the KO-X3 group with a significant increase in the 1–3 Hz range during the sleep-like state (Figure 6B; two-way ANOVA by frequency, genotype, and frequency × genotype and by post hoc Sidak multiple comparison; $p < 0.05$). This result suggested a restoration of the mechanism(s) that normally induces (induce) the increase in delta wave activity during sleep by AAV-X3 treatment and may suggest an improvement in sleep quality in these rats.

Wood chew and tube test

Male, but not female, *Fmr1* KO rats have been shown to engage in repetitive chewing behavior.[15] Therefore, the wood chew test was performed only in the male rats (Figure 7A). Although no significant differences were observed among treatment groups by one-way ANOVA ($p > 0.05$), the KOs injected with X3 showed a lower level of chewing compared with WTs injected with AAV-EV, whereas the KOs injected with AAV-EV displayed an intermediate effect. In addition, wood-chewing behavior was found to be increased in the WT-EV treatment group (median = 1.2, interquartile range [IQR] = 0.6–1.8) in comparison with data from uninjected male WT rats, which was reported in our earlier study (median = 0.4, IQR = 0.3–0.6).[15] This result suggests that injection of AAV-EV may have an effect on wood-chewing repetitive behavior and could be a confounding factor in this test.

Both male and female *Fmr1* KO rats were found to be more submissive compared with sex- and age-matched WT rats in the tube test of

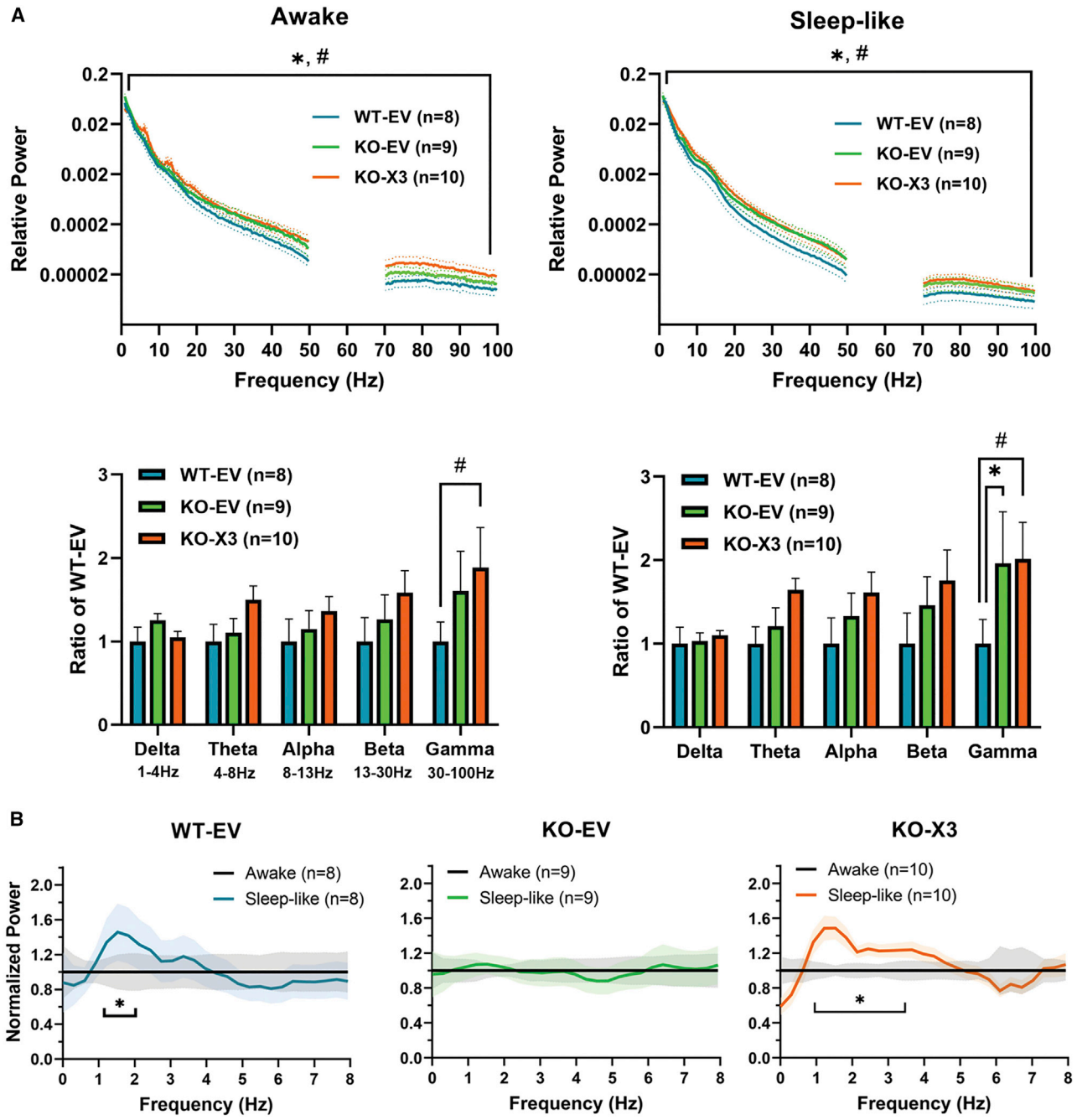

Figure 6. Effect of AAV-X3 treatment on EEG power spectrum in male *Fmr1* KO rats

(A) Power spectrum analyses and corresponding frequency band comparisons among the three treatment groups during awake and sleep states. * denotes significant difference ($p < 0.05$) between WT-EV and KO-EV, whereas # denotes significant difference ($p < 0.5$) between WT-EV and KO-X3. WT-EV was significantly different from KO-EV and KO-X3 by two-way ANOVA when the full spectrum (0–100 Hz) was compared. In the frequency band comparisons, post hoc analysis (Holm-Sidak multiple comparison test) revealed a significant increase in the gamma frequency range during the sleep-like state in the KO-EV group and during the awake and sleep-like states in the KO-X3 group. (B) Comparisons of slow wave power spectrum patterns among WT-EV, KO-EV, and KO-X3 treatment groups. The sleep-like state data (0–8 Hz) were normalized to the awake immobile state data. Significant increases (*) in the 1–2 Hz and 1–3 Hz frequency range using raw spectral power data were observed in the WT-EV and KO-X3 group, respectively (two-way ANOVA by frequency in the WT-EV group and by frequency, genotype and frequency × genotype in the KO-X3 group with post hoc Sidak multiple comparison; $p < 0.05$). The shaded area in each panel represents the SEM.

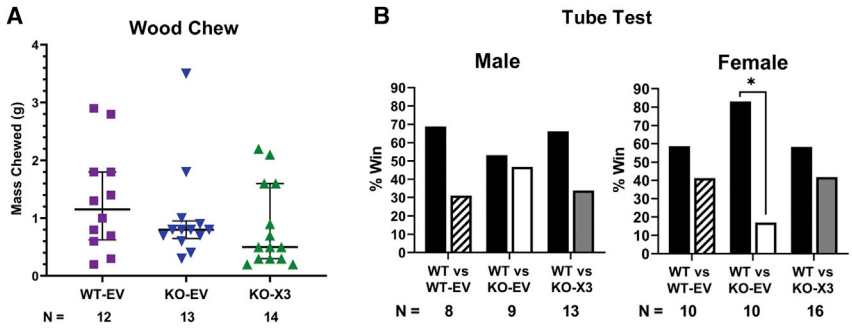

Figure 7. Results of the wood chew test and the tube test

(A) Results of the wood chew test in male (PND 65–70) *Fmr1* KO rats. Median ± interquartile range is shown. No statistically significant differences among treatment groups were observed by Kruskal-Wallis test ($p > 0.05$). (B) Tube test results from contests among untreated WT and WT-EV-, KO-EV-, and KO-X3-treated male and female rats (PND 49–54). The total number of wins from all the contests conducted in each group was combined. N = number of rats per group. Three contests were conducted for each pairing. Each treated rat was matched against 2.0 ± 0.1 WT opponents. * denotes significant difference ($p < 0.05$) by Fisher's exact test using the number of wins.

social dominance in our prior report on *Fmr1* KO rats.[15] Here, AAV-X3-treated male and female *Fmr1* KO rats both had a percentage of wins comparable to that of the WT rats treated with AAV-EV (Figure 7B). Female *Fmr1* KO rats treated with AAV-EV had significantly fewer wins against their WT opponent, consistent with previous results; however, that difference was not observed in the male KO-EV treatment group.[15] These results suggest that AAV-X3 treatment reversed the submissive behavioral phenotype in female *Fmr1* KO rats.

Open field test

We have previously demonstrated that *Fmr1* KO rats display reduced motor activity relative to WT controls in the open field test, with males demonstrating hypoactivity in the outer perimeter of the open field, whereas both male and female *Fmr1* KO rats were hypoactive in the center region of the field.[15] This was interpreted as an indication of elevated anxiety in the KOs in this test. Here, we examined the effect of AAV-X3 treatment on this endophenotype. No significant difference among treatments or genotypes was observed in the center area of the open field. However, consistent with our previous results in this line of *Fmr1* KO rat, *Fmr1* KO males injected with AAV-EV were found to be hypoactive across the total area of the open field and in the outer perimeter of the field (zone 1), relative to AAV-EV-injected WT rats (Figure 8A). A difference in activity was not observed for the total field area or in zone 1 between AAV-X3-treated *Fmr1* KO males and AAV-EV-treated WT males, indicating a partial rescue in activity by AAV-X3. No difference was observed between genotypes and treatments for female rats in the total area and in zone 1.

Fear conditioning test

Female *Fmr1* KO rats were reported to display an increased rate of freezing in response to a conditioned tone in the fear conditioning test, relative to WT females.[15] In AAV-treated *Fmr1* KO and WT rats, no difference was found between genotypes and treatments in response to the conditioned context (context A) or a novel context (context B; Figure 8B). *Fmr1* KO rats froze more than WT rats did, regardless of treatment, in response to the first minute of exposure to the conditioned tone. Correcting for inherent freezing activity on a per-animal basis (adjusted conditioned stimulus index = conditioned stimulus − context B) demonstrated a significant decrease in freezing during the third minute of exposure to the conditioned tone by *Fmr1* KO rats injected with AAV-X3, relative the *Fmr1* KO rats injected with AAV-EV. Treatment with AAV-X3 had no effect on the freezing rate of *Fmr1* KO rats in the first minute of exposure to the conditioned tone. Interestingly, *Fmr1* KO female rats injected with AAV-X3 showed a reduced freezing rate by the third minute of exposure to the conditioned tone (Figure 8B), which appears to be extinction of the fear response because excessive darting behavior was not seen during this period.

DISCUSSION

Anatomical and cellular distribution of the FMRP transgene

One goal of this study was to reproduce the WT spatial and temporal pattern of expression of FMRP in the *Fmr1* KO rat CNS. Using an injection protocol that combined ICV and ICM injections, we achieved widespread transduction throughout much of the telencephalon and diencephalon of rats and mice. However, transgene expression was more limited in the caudal regions of the brain, including the cerebellum and brainstem. The overall anatomical pattern of expression was generally reminiscent of our previous results in the mouse brain after ICV injection using mouse isoform 1 and a synapsin promoter.[6] In the current study, the purpose of combining the ICM injection with an ICV injection was to increase expression in the caudal regions of the brain. However, comparisons of ICV only with ICV+ICM indicated a relatively low to modest increase in FMRP expression in the caudal brain with the added ICM injection (results not shown).

Another operative factor could have been the anatomical activity of the mini-MeCP2 promoter in combination with the FMRP transgene. Like FMRP, MeCP2 is highly expressed in multiple neuronal types in the cerebellum.[23,24] Previous work examining LacZ expression in transgenic mice indicated that this version of the mini-MeCP2 promoter is capable of driving expression in Purkinje neurons in the mouse cerebellum at PNDs 7 and 24.[25] Although we observed a few transduced Purkinje neurons in the *Fmr1* KO rat and mouse brain, the level of FMRP expression was well below that seen in WT animals. Our previous experimentation in mice demonstrated that early postnatal ICV injection of AAV-FMRP driven by a synapsin promoter also showed low cerebellar expression.[5] In contrast, under the same

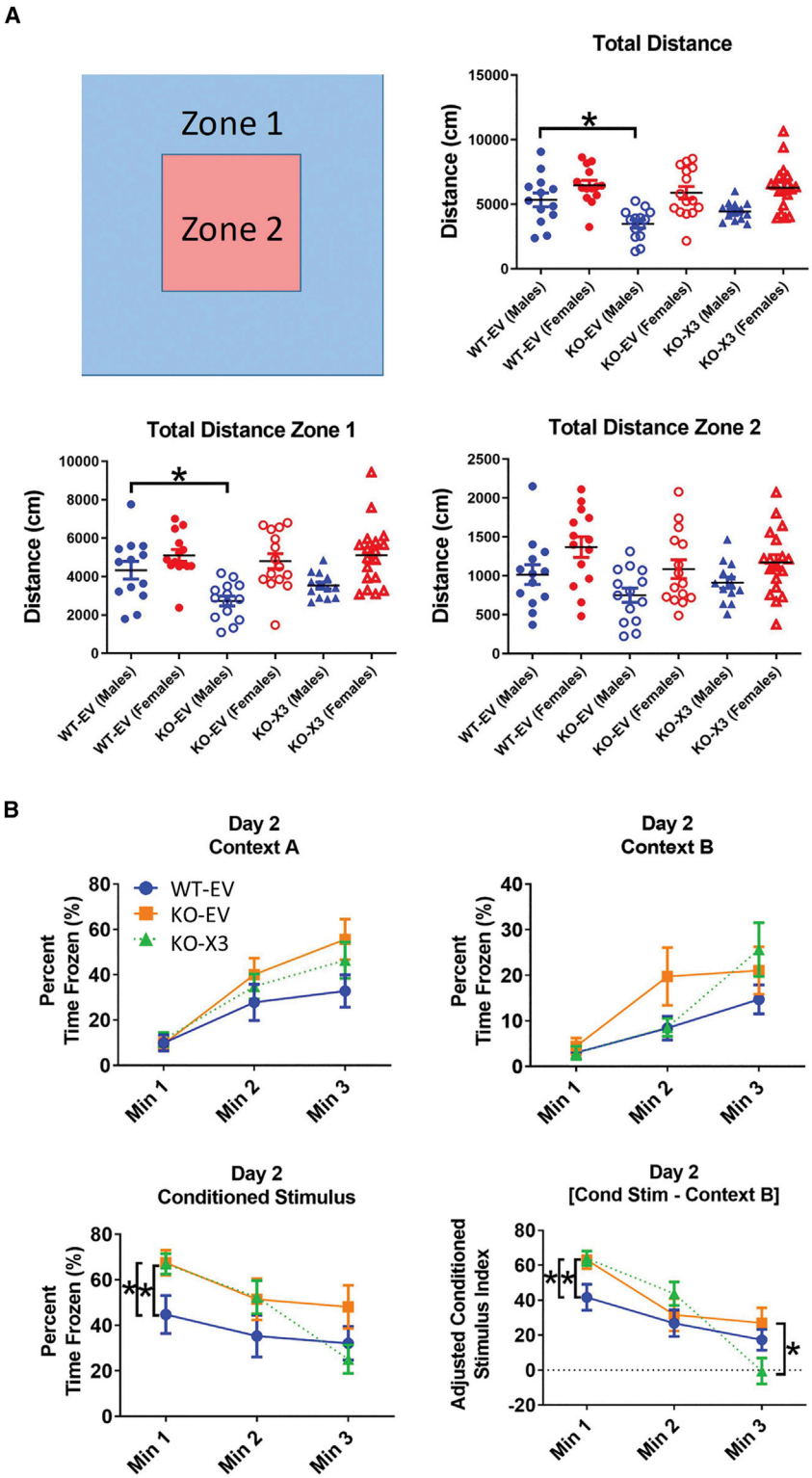

Figure 8. Behavioral analysis in the open field and fear conditioning tests

(A) Results of the open field test. *Fmr1* KO males injected with AAV-EV were significantly hypoactive in the total area of the open field and in the outer perimeter of the field (zone 1), relative to WT rats injected with AAV-EV. The hypoactivity was not observed in *Fmr1* KO males after treatment with AAV-X3. No difference was observed between genotypes and treatments for female rats. n-values: male: WT AAV-EV = 13, *Fmr1* KO AAV-EV = 14, *Fmr1* KO AAV-X3 = 13; female: WT AAV-EV = 14, *Fmr1* KO AAV-EV = 15, *Fmr1* KO AAV-X3 = 19. Error bars are means ± SEM. *$p < 0.05$ for two-way ANOVA and Tukey's post hoc. There was a significant effect of sex on the distance traveled in all zones tested ($p < 0.05$). (B) Results from the fear conditioning test. No difference was found between genotypes and treatments in response to the conditioned context (context A) or a novel context (context B). *Fmr1* KO rats froze more often than WT rats did, regardless of treatment, in response to the first minute of exposure to the conditioned tone. Correcting for inherent freezing activity on a per-animal basis (Cond Stim – context B) demonstrated a significant decrease in freezing during the third minute of exposure to the conditioned tone by *Fmr1* KO rats injected with AAV-X3, relative to the *Fmr1* KO rats injected with AAV-EV. N values: WT AAV-EV = 14, *Fmr1* KO AAV-EV = 15, *Fmr1* KO AAV-X3 = 19. Error bars are means ± SEM. *$p < 0.05$ for one-way ANOVA and Tukey's post hoc test comparing percentage of time frozen among groups at each time point.

injections conditions (early postnatal ICV injection), both the synapsin promoter or a cytomegalovirus (CMV) promoter gave robust expression of enhanced green fluorescent protein in the cerebellum.[26] We speculate that transduction levels achieved in different brain regions may be dependent not only on the timing of the injection and the dose injected but also on the precise combination of promoter and transgene.

Based on western blot analysis, a reduction of FMRP expression in the X3-injected KO rats was observed between PND 30 and PND 70 relative to WT levels at the same ages. Although the rat brain is still growing between these ages, the increase in brain size alone is likely not enough to account for the reduction in expression. Because there were no overt signs of cellular death or glial activation, it also seems unlikely that the transduced neurons were dying. In fact, the natural expression of FMRP in the mouse brain peaks between postnatal weeks 3 and 4, followed by a modest decline to a more steady-state level in the adult CNS.[24,27] Thus, the ontological activity of the mini-MeCP2 promoter may be similar to the endogenous *Fmr1* promoter.

Efficacy testing

Rats injected 2 days after birth were assessed for phenotypic correction as young adults between 6 and 10 weeks of age. The regimen for efficacy testing consisted of EEG analysis and an assessment on a battery of autism-related behavioral tests. Three treatment groups were compared: WT-EV, Fmr1 KO-EV, and Fmr1 KO-X3.

Motor hyperactivity is a salient feature of FXS in humans and *Fmr1* KO mice. However, our previous characterization of the *Fmr1* KO rat showed that the relative degree of motor activity was test dependent. We reported reduced distance traveled of the KOs compared with WT in the open field test but elevated motor activity in the home cage 24-h activity analysis.[15] The results of the former test, conducted over a 20-min period in a novel environment, suggested elevated anxiety in the untreated *Fmr1* KOs compared with WT rats, whereas the latter test was conducted over a 4-day period in the home cage, where the animals' natural hyperactivity was unmasked. In the current analysis of open field performance, male *Fmr1* KO rats injected with AAV-X3 had similar activity levels as WT rats injected with AAV-EV. On the other hand, *Fmr1* KO rats injected with AAV-EV were found to be hypoactive relative to the WT control group. That difference, taken with information that the mean activity of the *Fmr1* KO/AAV-X3 group is higher than that of the *Fmr1* KO/AAV-EV group, while having lower variability, indicates a partial rescue of the behavior. We speculate that full normalization of motor behavior may require FMRP expression in additional regions of the CNS. Despite rescue of other behaviors, treatment with AAV-X3 had little effect on fear conditioning. Fear conditioning relies on interaction between several brain regions, including the hippocampus, amygdala, cortex, and cerebellum.[28,29] Transduction of X3 in the hippocampus and amygdala was somewhat limited, indicating that prominent expression in the cerebral cortex alone was not sufficient to rescue that behavior.

Our previous EEG findings in untreated *Fmr1* KO rats demonstrated two salient abnormalities: an elevation in gamma power, and a reduction of delta frequency power in the sleep-like state compared with that of WT rats.[15] In AAV-treated *Fmr1* KO rats, we observed rescue of the delta power abnormality after AAV-X3 treatment but not the elevated gamma power. Delta waves are a marker of sleep homeostasis and are thought to be important in the consolidation of learning and memory.[30,31] Children with FXS experience sleep disturbances, including problems falling asleep and repeated night awakenings, and polysomnographic evaluations of boys with FXS revealed alterations in non-rapid eye movement (NREM) sleep microstructure.[32,33] Specifically, a decrease in transient slow oscillations in NREM sleep was observed, which have been related to intellectual disability.[32] Similarly, a reduction in slow delta frequency power was observed in *Fmr1* KO rats during the sleep-like state.[15] Our results suggest the possibility that AAV-X3 treatment may have improved sleep quality in the *Fmr1* KO rats.

An increase in EEG gamma frequency band power has been a consistent finding in patients with FXS compared with neurotypicals and in male *Fmr1* KO mice and rats compared with WTs.[15,18–21] This has been linked to an imbalance in excitation versus inhibition and neuronal hyperexcitability and has been hypothesized to underlie some of the behavioral disturbances observed in the disorder.[34–36] Gamma oscillations are thought to be generated by inhibitory interneurons; of which, fast-spiking PV^+ interneurons have an important role.[37–39] In *Fmr1* KO mice, impairments and reductions in the development, density, and activity of PV neurons have been reported.[40–42] Moreover, enhanced resting gamma oscillations in the auditory cortex of *Fmr1* KO mice appear to be mediated, in part, by PV interneurons via matrix metalloproteinase-9 (MMP-9)-dependent regulation of perineuronal nets.[43] The lack of correction of abnormal gamma power after AAV-X3 treatment in the *Fmr1* KO rats may suggest an insufficient expression of the FMRP transgene in these fast-spiking PV interneurons. That idea is consistent with the double-label immunostaining analysis (Figures 4 and S2) demonstrating low FMRP transgene expression in GABA and PV^+ interneurons. In addition to rectifying the gamma power abnormality, achieving higher FMRP expression in PV interneurons may also be required for a more comprehensive phenotypic correction.

Our findings demonstrate that AAV-mediated expression of the rat ortholog of a major human isoform of FMRP (isoform 17), rectified several behavioral and brain wave abnormalities in a rat model of FXS. These results, together with previous proof-of-concept studies of AAV-FMRP in the mouse model of FXS,[4–6] strengthen the validity of the FMRP replacement strategy for treating FXS. Nevertheless, additional technical improvements could provide a more holistic correction of the syndrome. As noted above, enhanced transduction of GABAergic interneurons would likely be beneficial, as would a modification in the protocol for drug administration that imparts viral transduction to caudal areas of the brain, including the cerebellum and brainstem, which have been linked to multiple FXS endophenotypes, such as language comprehension, altered affect, auditory processing deficits, and impaired cognitive function.[44–46] The reason for the

relatively low AAV-mediated FMRP expression in the caudal brain of the mouse and rat after intra-CSF injection is unknown, but might relate, in part, to the direction and capacity of CSF flow in rodents.[47] For translation to humans, the most commonly used intra-CSF injection procedure is intrathecal administration into the spinal canal. Recent studies in human subjects using real-time phase-contrast flow MRI have revealed that respiratory inhalation is a major driving force for conducting CSF upward toward the head.[48,49] This might explain, in part, the relatively prominent transduction of AAV-mediated viral expression in the non-human primate CNS[50–52] and may bode well for future assessment of AAV-FMRP in clinical trials.

MATERIALS AND METHODS

Rats and mice

WT and *Fmr1* KO mice on the C57BL/6 background, obtained from The Jackson Laboratory, were housed in groups of 3–4 with a 12-h light/12-h dark cycle. WT and *Fmr1* KO rats on the Long-Evans background strain were acquired and housed 2–3 per cage with a 12-h light/12-h dark cycle, as previously described by Wong et al.[15] All procedures with rodents were approved by the University of Toronto animal care committee.

AAV constructs

Three AAV9 vectors were used: AAV9-empty vector (AAV-EV), employing an AAV9 capsid but with no expressed transgene protein, was used as the baseline control; AAV9-mouse MeCP2 mini-promoter-mouse *Fmr1*-isoform 7 (AAV-iso7); and AAV9-rat MeCP2 mini-promoter-rat *Fmr1*-isoform X3 (AAV-X3; see Figure 1A). Rat isoform X3 and mouse isoform 7 are the orthologs of human isoform 17. All three AAVs contained the woodchuck hepatitis virus post-transcriptional regulatory element (WPRE) and a rabbit β-globin polyA tail. AAV9 FMRP vectors were generated following a scaled-down, research-grade version of a proprietary good manufacturing practices (GMP) vector production protocols at REGENXBIO (Rockville, MD). Briefly, suspension HEK293 cells (RGX293) were triple-transfected with the helper plasmid, AAV9 *trans*-plasmid, and the transgene plasmid containing either the rat FMRP isoform X3 or mouse FMRP isoform 7. The packaged vectors were purified from the cell culture supernatant using affinity chromatography and titered using Droplet Digital PCR (Bio-Rad, Hercules, CA, USA).

Drug administration

On PND 2 or 3, rats and mice were injected as described previously.[6,53] Mice were injected via bilateral ICV and ICM routes using custom-made 30-gauge needles. The sites of the needle insertion were 1 mm from the midline and 1 mm from lambda for ICV injection, and 2 mm from the lambda on the cerebellum along the midline for the ICM injection. The cut edge of the needle was directed rostrally for ICV injection and toward the dorsal side for ICM injection. The volume of the AAV vector was 1 μL/side for ICV injection, and 3 μL for ICM injection administered at a flow rate of 1 μL/min. The needle was left in place for additional 1 min after the infusion to avoid loss of the vector. Injections into PND 2 or 3 rats were also made via combined bilateral ICV + ICM. For ICV injections, the needle was inserted 2 mm deep, perpendicular to the skull surface, at a location approximately ±1.5 mm lateral to the sagittal suture, lateral from the bregma; the needle opening/bevel was directed rostrally. The needle tip was inserted through the skull using gentle pressure to penetrate the partially formed bony layer, and 4 μL of AAV9 vector was injected (i.e., 4 + 4 μL) into each side of ventricles at a flow rate of 1 μL/min. For ICM, the needle was inserted 2 mm deep at the base of the skull, angled toward the nose of the animal, and aligned with the midline of the brain with the needle opening pointing up toward the dorsal side of the skull. A total of 8 μL was injected ICM at a rate of 1 μL/min. The needle was left in place for an additional 1 min after the infusion.

Western blotting and immunocytochemical analyses

Western blots were carried out using 10% SDS-PAGE gels and transfers to nitrocellulose. The blots were probed with anti-FMRP antibodies (MMS-5232, BioLegend, CA, USA, 1:1,000; ab17722, Abcam, Cambridge, UK, 1:1,000), anti-Iba1 (016-20001, WAKO, Osaka, Japan, 1:1,000), anti-GFAP (75–240, NeuroMab, David, CA, USA, 1:1,000), or anti-GAPDH (ab9485, Abcam, Cambridge, UK, 1:5,000), and appropriate horseradish peroxidase (HRP) secondary antibodies (goat anti-mouse immunoglobulin G [IgG]-HRP, 115-035-003, Jackson ImmunoResearch, PA, USA, 1:2,000–1:4,000; goat anti-rabbit IgG-HRP, 111-035-003, Jackson ImmunoResearch, PA, USA, 1:2,000–1:4,000) and visualized on a Bio-Rad ChemiDoc imaging system or an Alpha Innotech imaging system, as described previously.[6,53]

For immunocytochemistry, mice and rats were anesthetized with ketamine/xylazine and perfused with ice-cold 1× PBS, followed by a 4% paraformaldehyde solution. The brains were incubated in the same fixative overnight at 4°C, followed by a 30% sucrose solution in PBS, and stored at 4°C; 30 μm sagittal sections of the brain were quenched in a 0.8% sodium borohydride solution for 5 min at room temperature. Samples were pooled from both sides of the brain at collection. After washing with PBS, the sections were incubated in blocking buffer (3% BSA, 5% donkey serum, or 5% goat serum, 0.2% Triton X-100, diluted with 1× PBS) for 1 h and then incubated overnight at 4°C in the primary antibody. Antigen retrieval was done in 0.1 M citrate buffer, pH 6.0, for 45 min. at 75°C. The following primary antibodies were used: mouse anti-FMRP, clone 5C2, was used for mouse brain sections (MMS-5232, Biolegend, CA, USA, 1:500), rabbit anti-FMRP (ab17722, Abcam, Cambridge, UK, 1:1,500) was used for rat brain sections, rabbit anti-NeuN (128886, Abcam, Cambridge, UK, 1:1,000), mouse anti-NeuN (MAB377, MilliporeSigma, MA, USA, 1:1,000), mouse anti-parvalbumin (PV) (P3088, MilliporeSigma, MA, USA, 1:1,000), rabbit anti-GAD65/67 (G5163, MilliporeSigma, MA, USA, 1:1,000), rabbit anti-S100B (ab868, Abcam, Cambridge, UK, 1:1,000), diluted in blocking solution. The sections were washed five times in PBS and incubated with the appropriate secondary antibodies, all from Jackson ImmunoResearch, PA, USA, and diluted 1:2,000–1:3,000: Alexa-Fluor-594-conjugated anti-rabbit IgG (no. 111-585-008), Alexa-Fluor-488-conjugated anti-rabbit IgG (cat. 111-545-008), Alexa-Fluor-594-conjugated anti-mouse IgG (no. 115-585-146), Alexa-Fluor-488-conjugated anti-mouse IgG (no. 115-545-146) diluted in blocking solution for 2 h, washed

five times, and incubated in DAPI (1:2,000) diluted in PBS, washed in PBS, and mounted on glass slides using ProLong Gold Antifade Mountant (P36930, Life Technologies, Carlsbad, CA, USA). Images were captured using an LSM710 confocal microscope (Zeiss, Germany) using 20× and 63× objective lenses, or using a BioTek Cytation 5 Cell Imaging Multi-Mode Reader (Bio-Rad) using 4× and 20× lenses. Microscope settings (pinhole, gain, and contrast) were kept constant for all the images in each experiment. Image analysis and quantification were carried out using FIJI.[54]

EEG recordings and data analyses

EEG recordings and analyses were conducted as described by Wong et al.[15] Briefly, two recording electrodes made of bipolar twisted polyimide-insulated stainless steel wires (Goodfellow Cambridge Limited, Huntington, UK) were implanted into the left and right rat frontal cortex (anterior/posterior: 4.7, medial/lateral: ±2.0) at a depth of ~2.0 mm. A reference electrode was placed epidurally on the occipital lobe (anterior/posterior: −6.0, medial/lateral: −2.0). During implantation surgery, three small holes ($\leq$0.5 mm) were drilled through the skull at these stereotaxic positions and after electrode placements, the electrodes were secured by dental acrylic (Jet Denture Repair Powder and Jet Acrylic Fluid, Lang Dental, Wheeling, IL, USA).

The EEG recordings took place between PND 40 and 55 (5–10 days after surgery). EEG signals were recorded using a differential AC amplifier (model 1700, A-M Systems, Carlsborg, WA, USA) and collected at an input frequency range of 0.1–1,000 Hz with amplification gain at 1,000×, and digitized at 5,000 Hz (Digidata 1550B, Axon Instruments/Molecular Devices, Union City, CA, USA). Each rat was recorded for 3 h in a Plexiglas recording chamber between 12:00 pm and 6:00 pm accompanied by video monitoring. Artifact-free epochs (>10 s) were selected only during immobility to minimize contamination by movement artifacts. "Immobile awake" state was defined as immobility accompanied by an upright head posture with eyes opened, whereas "immobile sleep-like" state was defined as immobility accompanied by the rat lying down in a prone position with its head down and eyes closed.

Data acquisition and analysis were performed using pCLAMP software version 11 (Axon Instruments/Molecular Devices). Fast Fourier transforms were run on each epoch using 0.3-Hz bins with 50% window overlap, and spectral power ($\mu V/Hz^2$) was calculated from 0 to 100 Hz. Spectral power from each state in the 3-h recording was combined for analysis. Relative power was calculated for each frequency band (delta: 1–4 Hz; theta: 4–8 Hz; alpha: 8–12 Hz; beta: 12–30 Hz; and gamma: 30–100 Hz) by dividing the spectral power of a given band by the total spectral power across the entire frequency spectrum (0–100 Hz). To visualize the change in delta power, spectral data from the sleep-immobile state were normalized to the awake immobile data (average group value) as normalized power. A 60-Hz notch filter was used to eliminate line noise, and frequencies from 50 to 70 Hz were excluded in all analyses. The investigator was blinded to the identity of the treatment groups during the recording and data extraction from individual rats.

Behavioral analyses

Open field test

Animals were tested in the open field, as previously described.[15] Briefly, the activity of PND 45–50 male and female rats was recorded for 20 min under low-light conditions (20 lux) in the 40 cm × 40 cm AccuScan locomotor activity testing apparatus (Omnitech Electronics, Columbus, OH, USA). All testing was performed between 1:00 and 6:00 pm. Activity was recorded with Fusion software (Omnitech Electronics, Columbus, OH, USA). Data were then split into 5-min bins for analysis. Data were also split into zones, in which zone 1 was the outer perimeter of the field, and zone 2 was the center area of the field, such that the width of zone 1 against any side was equal to half the width of the center area (zone 2).

Fear conditioning test

Fear conditioning was performed as previously described.[15] For all tests, animals were tested in a soundproof chamber using the Ugo Basile rat fear conditioning system with rat cage (no. 46002, Ugo Basile, Verase, Italy). Data and video were recorded using the accompanying ANYmaze software (version 6.06, Stoelting, IL, USA). All testing was performed between 1:00 and 6:00 pm with white noise and lighting in the chamber. Fear conditioning consisted of a 2-day protocol as described, with conditioning/training on the first day, and the second day consisting of measuring of the conditioning response to the original conditioned context (context A), a novel context (context B), and to the conditioned tone presented in context B, for 3 min each.

Wood chew test

The wood chew test was performed as described by Wong et al.[15] in male WT and *Fmr1* KO rats (PND 65–70). Briefly, rats were single housed from 16:00 to 09:00 hours in a clean cage with standard bedding and a 1 in × 1 in × 1-in wood block. The wood block was weighed before and after exposure, and the difference in weight was calculated as mass chewed (g).

Tube test for social dominance

The tube test was performed as described, between PNDs 49 and 54.[15] A transparent Plexiglas tube of 1 m in length was placed between two clean rat cages. Tubes of different internal diameter (7 cm and 6 cm) were used for the male and female rats, respectively. Rats were able to move freely but were unable to turn around or pass each other inside the tube. *Fmr1* KO rats were matched against an age- and sex-matched wild-type opponent that they had never been housed together with. Opponents were placed into their respective ends of the tube simultaneously and the match ended when one rat had both of its hind paws outside of the tube. The rat remaining in the tube was deemed the winner. Each matched pair was tested three times. The number of wins for each group was combined and Fisher's exact test was used to determine whether the percentage of wins in each group was significantly different from the 50:50 win/loss outcome expected by chance.

SUPPLEMENTAL INFORMATION

Supplemental information can be found online at https://doi.org/10.1016/j.omtm.2021.06.013.

ACKNOWLEDGMENTS

The authors are grateful for financial support from REGENXBIO, the Fragile X Research Foundation of Canada, and the Canadian Institutes for Health Research. We thank Azadeh Bazarchi, Bonnie Wu, Amanda Zhang, Timur Gaynutinov, and Ayda Myer for their excellent support with AAV vector production and Sara Berl, Laura Coruzzi, Stacey Curtiss, and Mary Johnson for helpful comments on the manuscript.

AUTHOR CONTRIBUTIONS

D.R.H., A.W.M.H., H.W., J.T.B., S.K.-M., and O.D. conceived the project; A.W.M.H., H.W., Y.N., R.A., and C.Q. conducted the experiments; D.R.H., A.W.M.H., H.W., Y.N., and R.A. analyzed the data. D.R.H., A.W.M.H., and H.W. wrote the first draft of the manuscript, followed by input from all other authors.

DECLARATION OF INTERESTS

S.K.-M., O.D., and J.T.B. declare that they own stock in and are employees of REGENXBIO. All other authors declare no conflicts of interest.

REFERENCES

1. Hagerman, P.J. (2008). The fragile X prevalence paradox. J. Med. Genet. *45*, 498–499.
2. Hunter, J., Rivero-Arias, O., Angelov, A., Kim, E., Fotheringham, I., and Leal, J. (2014). Epidemiology of fragile X syndrome: a systematic review and meta-analysis. Am. J. Med. Genet. A. *164A*, 1648–1658.
3. Hampson, D.R., Hooper, A.W.M., and Niibori, Y. (2019). The application of adeno-associated viral vector gene therapy to the treatment of fragile X syndrome. Brain Sci. *9*, 32.
4. Zeier, Z., Kumar, A., Bodhinathan, K., Feller, J.A., Foster, T.C., and Bloom, D.C. (2009). Fragile X mental retardation protein replacement restores hippocampal synaptic function in a mouse model of fragile X syndrome. Gene Ther. *16*, 1122–1129.
5. Gholizadeh, S., Arsenault, J., Xuan, I.C., Pacey, L.K., and Hampson, D.R. (2014). Reduced phenotypic severity following adeno-associated virus-mediated Fmr1 gene delivery in fragile X mice. Neuropsychopharmacology *39*, 3100–3111.
6. Arsenault, J., Gholizadeh, S., Niibori, Y., Pacey, L.K., Halder, S.K., Koxhioni, E., Konno, A., Hirai, H., and Hampson, D.R. (2016). FMRP expression levels in mouse central nervous system neurons determine behavioral phenotype. Hum. Gene Ther. *27*, 982–996.
7. Khandjian, E.W., Fortin, A., Thibodeau, A., Tremblay, S., Côté, F., Devys, D., Mandel, J.L., and Rousseau, F. (1995). A heterogeneous set of FMR1 proteins is widely distributed in mouse tissues and is modulated in cell culture. Hum. Mol. Genet. *4*, 783–789.
8. Sittler, A., Devys, D., Weber, C., and Mandel, J.L. (1996). Alternative splicing of exon 14 determines nuclear or cytoplasmic localisation of fmr1 protein isoforms. Hum. Mol. Genet. *5*, 95–102.
9. Brackett, D.M., Qing, F., Amieux, P.S., Sellers, D.L., Horner, P.J., and Morris, D.R. (2013). FMR1 transcript isoforms: association with polyribosomes; regional and developmental expression in mouse brain. PLoS ONE *8*, e58296.
10. Fu, X., Zheng, D., Liao, J., Li, Q., Lin, Y., Zhang, D., Yan, A., and Lan, F. (2015). Alternatively spliced products lacking exon 12 dominate the expression of fragile X mental retardation 1 gene in human tissues. Mol. Med. Rep. *12*, 1957–1962.
11. Pretto, D.I., Eid, J.S., Yrigollen, C.M., Tang, H.T., Loomis, E.W., Raske, C., Durbin-Johnson, B., Hagerman, P.J., and Tassone, F. (2015). Differential increases of specific FMR1 mRNA isoforms in premutation carriers. J. Med. Genet. *52*, 42–52.
12. Dury, A.Y., El Fatimy, R., Tremblay, S., Rose, T.M., Côté, J., De Koninck, P., and Khandjian, E.W. (2013). Nuclear fragile X mental retardation protein is localized to Cajal bodies. PLoS Genet. *9*, e1003890.
13. Ellenbroek, B., and Youn, J. (2016). Rodent models in neuroscience research: is it a rat race? Dis. Model. Mech. *9*, 1079–1087.
14. Szpirer, C. (2020). Rat models of human diseases and related phenotypes: a systematic inventory of the causative genes. J. Biomed. Sci. *27*, 84.
15. Wong, H., Hooper, A.W.M., Niibori, Y., Lee, S.J., Hategan, L.A., Zhang, L., Karumuthil-Melethil, S., Till, S.M., Kind, P.C., Danos, O., et al. (2020). Sexually dimorphic patterns in electroencephalography power spectrum and autism-related behaviors in a rat model of fragile X syndrome. Neurobiol. Dis. *146*, 105118.
16. Arsenault, J., Hooper, A.W.M., Gholizadeh, S., Kong, T., Pacey, L.K., Koxhioni, E., Niibori, Y., Eubanks, J.H., Wang, L.Y., and Hampson, D.R. (2021). Interregulation between fragile X mental retardation protein and methyl CpG binding protein 2 in the mouse posterior cerebral cortex. Hum. Mol. Genet. *29*, 3744–3756.
17. Gholizadeh, S., Halder, S.K., and Hampson, D.R. (2015). Expression of fragile X mental retardation protein in neurons and glia of the developing and adult mouse brain. Brain Res. *1596*, 22–30.
18. Ethridge, L.E., White, S.P., Mosconi, M.W., Wang, J., Pedapati, E.V., Erickson, C.A., Byerly, M.J., and Sweeney, J.A. (2017). Neural synchronization deficits linked to cortical hyper-excitability and auditory hypersensitivity in fragile X syndrome. Mol. Autism *8*, 22.
19. Lovelace, J.W., Ethell, I.M., Binder, D.K., and Razak, K.A. (2018). Translation-relevant EEG phenotypes in a mouse model of Fragile X Syndrome. Neurobiol. Dis. *115*, 39–48.
20. Sinclair, D., Featherstone, R., Naschek, M., Nam, J., Du, A., Wright, S., Pance, K., Melnychenko, O., Weger, R., Akuzawa, S., et al. (2017). GABA-B agonist baclofen normalizes auditory-evoked neural oscillations and behavioral deficits in the Fmr1 knockout mouse model of fragile X syndrome. eNeuro *4*, ENEURO.0380-16.2017.
21. Wang, J., Ethridge, L.E., Mosconi, M.W., White, S.P., Binder, D.K., Pedapati, E.V., Erickson, C.A., Byerly, M.J., and Sweeney, J.A. (2017). A resting EEG study of neocortical hyperexcitability and altered functional connectivity in fragile X syndrome. J. Neurodev. Disord. *9*, 11.
22. Kozono, N., Okamura, A., Honda, S., Matsumoto, M., and Mihara, T. (2020). Gamma power abnormalities in a Fmr1-targeted transgenic rat model of fragile X syndrome. Sci. Rep. *10*, 18799.
23. Olson, C.O., Zachariah, R.M., Ezeonwuka, C.D., Liyanage, V.R., and Rastegar, M. (2014). Brain region-specific expression of MeCP2 isoforms correlates with DNA methylation within Mecp2 regulatory elements. PLoS ONE *9*, e90645.
24. Pacey, L.K., Xuan, I.C., Guan, S., Sussman, D., Henkelman, R.M., Chen, Y., Thomsen, C., and Hampson, D.R. (2013). Delayed myelination in a mouse model of fragile X syndrome. Hum. Mol. Genet. *22*, 3920–3930.
25. Adachi, M., Keefer, E.W., and Jones, F.S. (2005). A segment of the Mecp2 promoter is sufficient to drive expression in neurons. Hum. Mol. Genet. *14*, 3709–3722.
26. Gholizadeh, S., Tharmalingam, S., Macaldaz, M.E., and Hampson, D.R. (2013). Transduction of the central nervous system after intracerebroventricular injection of adeno-associated viral vectors in neonatal and juvenile mice. Hum. Gene Ther. Methods *24*, 205–213.
27. Bonaccorso, C.M., Spatuzza, M., Di Marco, B., Gloria, A., Barrancotto, G., Cupo, A., Musumeci, S.A., D'Antoni, S., Bardoni, B., and Catania, M.V. (2015). Fragile X mental retardation protein (FMRP) interacting proteins exhibit different expression patterns during development. Int. J. Dev. Neurosci. *42*, 15–23.
28. Chaaya, N., Battle, A.R., and Johnson, L.R. (2018). An update on contextual fear memory mechanisms: transition between amygdala and hippocampus. Neurosci. Biobehav. Rev. *92*, 43–54.
29. Sacchetti, B., Scelfo, B., and Strata, P. (2005). The cerebellum: synaptic changes and fear conditioning. Neuroscientist *11*, 217–227.
30. Bellesi, M., Riedner, B.A., Garcia-Molina, G.N., Cirelli, C., and Tononi, G. (2014). Enhancement of sleep slow waves: underlying mechanisms and practical consequences. Front. Syst. Neurosci. *8*, 208.
31. Hobson, J.A., and Pace-Schott, E.F. (2002). The cognitive neuroscience of sleep: neuronal systems, consciousness and learning. Nat. Rev. Neurosci. *3*, 679–693.
32. Miano, S., Bruni, O., Elia, M., Scifo, L., Smerieri, A., Trovato, A., Verrillo, E., Terzano, M.G., and Ferri, R. (2008). Sleep phenotypes of intellectual disability: a

polysomnographic evaluation in subjects with Down syndrome and fragile-X syndrome. Clin. Neurophysiol. *119*, 1242–1247.

33. Kronk, R., Bishop, E.E., Raspa, M., Bickel, J.O., Mandel, D.A., and Bailey, D.B., Jr. (2010). Prevalence, nature, and correlates of sleep problems among children with fragile X syndrome based on a large scale parent survey. Sleep *33*, 679–687.
34. Cea-Del Rio, C.A., and Huntsman, M.M. (2014). The contribution of inhibitory interneurons to circuit dysfunction in Fragile X Syndrome. Front. Cell. Neurosci. *8*, 245.
35. Gonçalves, J.T., Anstey, J.E., Golshani, P., and Portera-Cailliau, C. (2013). Circuit level defects in the developing neocortex of Fragile X mice. Nat. Neurosci. *16*, 903–909.
36. Mably, A.J., and Colgin, L.L. (2018). Gamma oscillations in cognitive disorders. Curr. Opin. Neurobiol. *52*, 182–187.
37. Sohal, V.S., Zhang, F., Yizhar, O., and Deisseroth, K. (2009). Parvalbumin neurons and gamma rhythms enhance cortical circuit performance. Nature *459*, 698–702.
38. Cardin, J.A., Carlén, M., Meletis, K., Knoblich, U., Zhang, F., Deisseroth, K., Tsai, L.H., and Moore, C.I. (2009). Driving fast-spiking cells induces gamma rhythm and controls sensory responses. Nature *459*, 663–667.
39. Fröhlich, F. (2016). Gamma oscillations. In Network Neuroscience, *Chapter 21*, F. Fröhlich, ed. (Academic Press), pp. 271–280.
40. Selby, L., Zhang, C., and Sun, Q.Q. (2007). Major defects in neocortical GABAergic inhibitory circuits in mice lacking the fragile X mental retardation protein. Neurosci. Lett. *412*, 227–232.
41. Wen, T.H., Afroz, S., Reinhard, S.M., Palacios, A.R., Tapia, K., Binder, D.K., Razak, K.A., and Ethell, I.M. (2018). Genetic reduction of matrix metalloproteinase-9 promotes formation of perineuronal nets around parvalbumin-expressing interneurons and normalizes auditory cortex responses in developing Fmr1 knock-out mice. Cereb. Cortex *28*, 3951–3964.
42. Goel, A., Cantu, D.A., Guilfoyle, J., Chaudhari, G.R., Newadkar, A., Todisco, B., de Alba, D., Kourdougli, N., Schmitt, L.M., Pedapati, E., et al. (2018). Impaired perceptual learning in a mouse model of fragile X syndrome is mediated by parvalbumin neuron dysfunction and is reversible. Nat. Neurosci. *21*, 1404–1411.
43. Lovelace, J.W., Rais, M., Palacios, A.R., Shuai, X.S., Bishay, S., Popa, O., Pirbhoy, P.S., Binder, D.K., Nelson, D.L., Ethell, I.M., and Razak, K.A. (2020). Deletion of Fmr1 from forebrain excitatory neurons triggers abnormal cellular, eeg, and behavioral phenotypes in the auditory cortex of a mouse model of fragile X Syndrome. Cereb. Cortex *30*, 969–988.
44. Hampson, D.R., and Blatt, G.J. (2015). Autism spectrum disorders and neuropathology of the cerebellum. Front. Neurosci. *9*, 420.
45. Yang, Y.M., Arsenault, J., Bah, A., Krzeminski, M., Fekete, A., Chao, O.Y., Pacey, L.K., Wang, A., Forman-Kay, J., Hampson, D.R., and Wang, L.Y. (2020). Identification of a molecular locus for normalizing dysregulated GABA release from interneurons in the fragile X brain. Mol. Psychiatry *25*, 2017–2035.
46. McCullagh, E.A., Rotschafer, S.E., Auerbach, B.D., Klug, A., Kaczmarek, L.K., Cramer, K.S., Kulesza, R.J., Jr., Razak, K.A., Lovelace, J.W., Lu, Y., et al. (2020). Mechanisms underlying auditory processing deficits in fragile X syndrome. FASEB J. *34*, 3501–3518.
47. Faubel, R., Westendorf, C., Bodenschatz, E., and Eichele, G. (2016). Cilia-based flow network in the brain ventricles. Science *353*, 176–178.
48. Dreha-Kulaczewski, S., Joseph, A.A., Merboldt, K.D., Ludwig, H.C., Gärtner, J., and Frahm, J. (2017). Identification of the upward movement of human CSF *in vivo* and its relation to the brain venous system. J. Neurosci. *37*, 2395–2402.
49. Dreha-Kulaczewski, S., Konopka, M., Joseph, A.A., Kollmeier, J., Merboldt, K.D., Ludwig, H.C., Gärtner, J., and Frahm, J. (2018). Respiration and the watershed of spinal CSF flow in humans. Sci. Rep. *8*, 5594.
50. Passini, M.A., Bu, J., Richards, A.M., Treleaven, C.M., Sullivan, J.A., O'Riordan, C.R., Scaria, A., Kells, A.P., Samaranch, L., San Sebastian, W., et al. (2014). Translational fidelity of intrathecal delivery of self-complementary AAV9-survival motor neuron 1 for spinal muscular atrophy. Hum. Gene Ther. *25*, 619–630.
51. Meyer, K., Ferraiuolo, L., Schmelzer, L., Braun, L., McGovern, V., Likhite, S., Michels, O., Govoni, A., Fitzgerald, J., Morales, P., et al. (2015). Improving single injection CSF delivery of AAV9-mediated gene therapy for SMA: a dose-response study in mice and nonhuman primates. Mol. Ther. *23*, 477–487.
52. Samaranch, L., Pérez-Cañamás, A., Soto-Huelin, B., Sudhakar, V., Jurado-Arjona, J., Hadaczek, P., Ávila, J., Bringas, J.R., Casas, J., Chen, H., et al. (2019). Adeno-associated viral vector serotype 9-based gene therapy for Niemann-Pick disease type A. Sci. Transl. Med. *11*, eaat3738.
53. Niibori, Y., Lee, S.J., Minassian, B.A., and Hampson, D.R. (2020). Sexually divergent mortality and partial phenotypic rescue after gene therapy in a mouse model of dravet syndrome. Hum. Gene Ther. *31*, 339–351.
54. Schindelin, J., Arganda-Carreras, I., Frise, E., Kaynig, V., Longair, M., Pietzsch, T., Preibisch, S., Rueden, C., Saalfeld, S., Schmid, B., et al. (2012). Fiji: an open-source platform for biological-image analysis. Nat. Methods *9*, 676–682.